https://doi.org/10.5194/egusphere-2026-2220
Preprint. Discussion started: 23 April 2026

Multiple microscale stable isotope signatures record metabolic processes in ancient deep subsurface barite-pyrite-calcite assemblages

Eric Runge[1,2*], Vanessa Fichtner[1,3], Mikael Tillberg[1], Martin Whitehouse[4], Henrik Drake[1]

[1]Department of Biology and Environmental Science, Linnaeus University, Kalmar, Sweden
[2]GeoZentrum Nordbayern, Friedrich-Alexander Universität (FAU) Erlangen-Nürnberg, Erlangen, Germany
[3]Department of Geobiology, University of Göttingen, Göttingen, Germany
[4]Laboratory for Isotope Geology, Swedish Museum of Natural History, Stockholm, Sweden

Correspondence to: Eric Runge (eric.runge@fau.de)

Abstract. Fracture-coating pyrite from deep within the Fennoscandian Shield records the largest ^{34}S-enrichment observed on Earth to date ($\delta^{34}S = +147$ ‰) – likely the result of late-stage Rayleigh distillation during closed-system microbial sulfate reduction (MSR). This implies even heavier sulfur isotope values for the complementary sulfate reservoir during pyrite formation, possibly recorded in coeval sulfate minerals such as barite [$BaSO_4$]. However, barite has been poorly explored as an archive of ancient deep subsurface biosignatures. Here, we compiled published microscale $\delta^{34}S_{pyrite}$, $\delta^{18}O_{calcite}$, and $\delta^{13}C_{calcite}$ data with new secondary ion mass spectrometry (SIMS) $\delta^{34}S_{barite}$ and $\delta^{18}O_{barite}$ analyses from two localities on the Fennoscandian Shield (Forsmark and Laxemar/ Äspö, Southeastern Sweden), aiming to constrain how barite records the history of microbial processes. Comparison between the $\delta^{34}S_{pyrite}$ range across both localities (−53.9 to +131.7 ‰) with the $\delta^{34}S_{barite}$ range (+7.6 to +52.0 ‰) demonstrates that the sulfate reservoir corresponding to extremely ^{34}S-enriched pyrite is not recorded in barite. We identified two groups of barite distinguished by their distinct $\delta^{18}O$/ $\delta^{34}S$ trends, which is proposed to record different MSR-related processes based on cogenetic $\delta^{13}C_{calcite}$ data. Although there is overlap between the metabolic processes recorded in both groups, the steeper trending Group 1 was dominantly associated with sulfate-dependent anaerobic oxidation of methane (AOM), whereas the shallower trending Group 2 was dominated by organoclastic sulfate reduction (OSR). The different trends likely resulted from an interplay of MSR pathways (AOM vs. OSR), as well as variations in sulfate reduction rates (SRR) and fractionation-related isotope enrichment ($^{34}\varepsilon$), attributed to paleoenvironmental ratios of sulfate to electron donor abundances. Lower sulfate/ electron donor ratios favored methanogenesis and AOM at lower SRR, whereas higher ratios inhibited methanogenesis and favored OSR at higher SRR. A preservation bias against extremely ^{34}S-enriched barite due to undersaturation at high degrees of Rayleigh distillation likely explains its absence in the deep subsurface. Our study highlights the need for microscale multiple stable isotope signatures in fracture-hosted mineral assemblages to understand metabolic processes in the ancient deep biosphere, while stressing that these records are strongly affected by local hydrogeochemical conditions.

1 Introduction

Fractures and rock pores in the continental crust represent one of the largest habitable environments on Earth. The average depth of the 122 °C isotherm, the upper known temperature limit of life (Takai et al., 2008), in the continental crust is 4.8 km, implying a vast habitable rock volume (Magnabosco et al., 2018). This 'deep biosphere' hosts diverse communities of chemolithoautotrophic primary producers and heterotrophic microorganisms, including methanogens, methanotrophs, and sulfate reducers (Chivian et al., 2008; Kieft et al., 2018; Ruff et al., 2024; Stevens and McKinley, 1995; Wu et al., 2016). Recent estimates of the total biomass of the deep biosphere vary (Bar-On et al., 2018; Magnabosco et al., 2018; McMahon and Parnell, 2014), but its significant impact on global biogeochemical cycles is generally accepted. It has been suggested that the deep subsurface may have held the majority of Earth's total biomass before the rise of land plants (McMahon and Parnell, 2018). Indeed, portions of the continental crust have been continuously habitable for up to 1.1 billion years and may have experienced habitable time windows since 1.9 billion years ago (Ga) (Drake and Reiners, 2021). Understanding the diversity and biogeochemical impact of the deep biosphere throughout Earth's history requires robust and geologically stable biosignatures. However, the deep biosphere fossil record remains patchy and poorly understood (Gustafsson and Drake, 2025; Ivarsson et al., 2020).

Minerals and their stable isotope ratios can represent valuable biosignatures in deep time (Runge et al., 2023). For instance, the largest magnitudes of sulfur isotope fractionation ($^{34}\varepsilon = \delta^{34}S_{SO4}–\delta^{34}S_{H2S}$) are associated with kinetic isotope effects during microbial sulfate reduction (MSR). Depending on the microbial strain and environmental parameters, such as the availability of sulfate and electron donors (organic matter or H_2) or temperature, $^{34}\varepsilon$ induced by MSR can vary between 0 and ~70 ‰ (Bradley et al., 2016; Chambers et al., 1975; Farquhar et al., 2003; Habicht et al., 2002; Ries et al., 2009; Sim et al., 2011; Wing and Halevy, 2014; Wortmann et al., 2001). These signatures can be recorded in ^{34}S-depleted authigenic sulfide minerals (e.g., pyrite) (Halevy et al., 2023; Pasquier et al., 2025; Strauss, 1997). Thermochemical sulfate reduction (TSR) becomes dominant at temperatures exceeding 100 °C and can involve sulfur isotope fractionation via a kinetic isotope effect (KIE) at up to $\Delta^{34}S_{SO4–H2S} \approx 20$ ‰ at 100 °C; Kiyosu and Krouse, 1990; Machel et al., 1995). Equilibrium fractionation at 100 °C could reach $\Delta^{34}S_{SO4–H2S} \approx 43$ ‰ (Eldridge et al., 2016), representing a theoretical maximum for TSR.

Microbial sulfate reduction can also be coupled with sulfate-dependent anaerobic oxidation of methane (AOM), which is well supported in the deep subsurface (Bell et al., 2022; Drake et al., 2015a, 2017; Kotelnikova, 2002). Methane is typically ^{13}C-depleted because microbial methanogenesis induces strong carbon isotope fractionation ($^{13}\varepsilon = \delta^{13}C_{CO2}–\delta^{13}C_{CH4} \approx 95$ ‰; Whiticar, 1999). This can lead to ^{13}C-enrichment in the residual inorganic carbon pool or be recorded as strongly ^{13}C-depleted authigenic carbonates (e.g., calcite) as a result of methane oxidation (Aloisi et al., 2002; Campbell et al., 2002; Feng et al., 2010; Lin et al., 2011; Natalicchio et al., 2012; Reitner et al., 2005). During organoclastic sulfate reduction (OSR; i.e., MSR coupled to the oxidation of organic substrates) and AOM, the $\delta^{18}O$ of residual sulfate increases via a minor kinetic isotope effect and equilibration between intermediate sulfur species and $\delta^{18}O_{H2O}$ (Antler et al., 2013; Böttcher et al., 1999;

Brunner et al., 2005; Fritz et al., 1989; Mizutani and Rafter, 1973; Wortmann et al., 2007). Thus, the combination of sulfur, carbon, and oxygen isotope ratios is a powerful approach for reconstructing ancient MSR in these settings.

The slopes of $\delta^{18}O_{SO4}$/ $\delta^{34}S_{SO4}$ trends during the early stages of MSR is primarily controlled by the fraction of intermediate sulfur species (enzymatically-activated sulfate (APS) and sulfite) that are intracellularly re-oxidized to sulfate (Antler et al., 2013; Brunner et al., 2005; Wortmann et al., 2007) (Fig. 1). This fraction is strongly controlled by the cell-specific sulfate reduction rate (SRR). At a lower SRR, a higher fraction of sulfur intermediates is oxidized, leading to greater equilibration with $\delta^{18}O_{H2O}$ and a stronger increase in $\delta^{18}O_{SO4}$ relative to $\delta^{34}S_{SO4}$ (i.e., a steeper trend). At a higher SRR, a lower fraction of sulfur intermediates is oxidized, leading to stronger increase of $\delta^{34}S_{SO4}$ relative to $\delta^{18}O_{SO4}$ (i.e., a shallower trend). Sulfate reduction rates in the deep subsurface are generally low (Hoehler and Jørgensen, 2013), but relative variations in SRR may result from differences in temperature, abundance of sulfate-reducing microorganisms, competition with other microorganisms, availability of electron donors, quality of organic substrates, and sulfate concentrations (Boudreau and Westrich, 1984; Pallud and Van Cappellen, 2006; Roychoudhury et al., 2003). In addition, AOM and OSR can produce different trends at similar SRR (Antler et al., 2014). The trends produced by AOM differ between methane diffusion-limited settings (e.g., marine sediments: steeper trend) and methane-in-excess environments (e.g., gas seeps, stratified estuaries: shallower trend) (Antler et al., 2015) (Fig. 1). Owing to the preferential consumption of $^{32}SO_4^{2-}$ by microorganisms, MSR in a closed system (i.e., when total sulfate reduction rates exceed the resupply of sulfate) can produce ^{34}S-enriched sulfate in the residual porewater (Drake et al., 2018; Jørgensen et al., 2004; Paiste et al., 2022; Rudnicki et al., 2001; Zaback et al., 1993). In extreme cases, this process has produced $\delta^{34}S_{pyrite}$ values of up to +147 ‰ in deep fracture systems of the Fennoscandian Shield, the largest ^{34}S-enrichment yet reported (Drake et al., 2018). This implies an even more ^{34}S-enriched complementary sulfate reservoir, which may be recorded by coeval and geologically stable sulfate minerals.

Barite [$BaSO_4$] is a robust archive of $\delta^{34}S_{SO4}$ and $\delta^{18}O_{SO4}$ values in its parent fluid because i) its precipitation is associated with minimal stable isotope fractionation and ii) it can resist diagenetic and metamorphic overprints over geological time (Crockford et al., 2019; Griffith and Paytan, 2012; Han et al., 2025; Paytan et al., 1998, 2002; Turchyn and Schrag, 2004, 2006). Notably, ^{34}S-enriched barite is a commonly used proxy for the paleostratigraphic position of the sulfate-methane transition zone (SMTZ) in sedimentary environments, where barite forms under sulfate-limited conditions affected by AOM (Torres et al., 1996; Wood et al., 2021; Yang et al., 2023; Zan et al., 2022; Zhou et al., 2015). Stable isotope analysis of recently precipitated minerals on drill core equipment from the Äspö Hard Rock Laboratory (Sweden) indicated that combining pyrite and barite records is a promising approach for interpreting biosignatures in the deep subsurface (Fichtner et al., 2024). Thus, the co-variation of δ^{34}S and δ^{18}O in barite may record past and extant environmental conditions and microbial sulfur cycling. Notably, dating of fracture-coating minerals (adularia Rb/Sr, calcite U/Pb, and hematite U-Th/He) co-genetic to calcite- and pyrite-hosted stable isotope biosignatures of OSR and AOM deep in the Fennoscandian Shield between the Ordovician (460 ± 30 Ma) and the Neogene (13.7 ± 0.6 Ma) (Drake et al., 2017, 2018, 2021). However, barite has been poorly explored as an ancient archive for deep subsurface microbial processes.

Here, we compile new secondary ion mass spectrometry (SIMS) $\delta^{18}O_{barite}$ and $\delta^{34}S_{barite}$ data from multiple deep drill cores taken at two localities on the Fennoscandian Shield (Forsmark and Laxemar/ Äspö, Southeastern Sweden) with previously published $\delta^{13}C_{calcite}$, $\delta^{18}O_{calcite}$, and $\delta^{34}S_{pyrite}$ data from the same drill cores. In most cases, barite could be correlated with pyrite and/or calcite from the same fracture. Although we did not find extremely ^{34}S-enriched barite in our samples, the barite records an ancient archive of OSR and AOM. These biosignature records are strongly controlled by local paleoenvironmental conditions. We suggest that a preservation bias against superheavy barite contributes to their absence in the geological record.

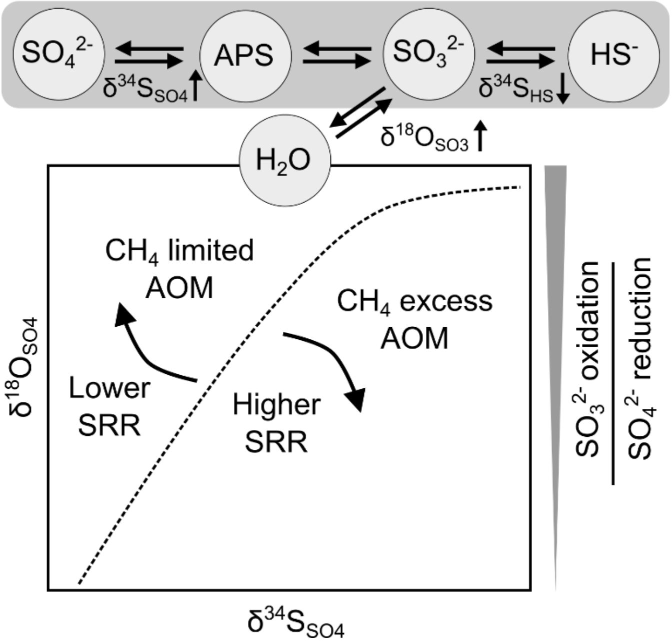

Figure 1: Controls on $\delta^{18}O_{SO4}$-$\delta^{34}S_{SO4}$ trends in residual sulfate (SO_4^{2-}) during the early stages of microbial sulfate reduction (MSR). The intracellular reduction of sulfate to sulfide (HS^-), proceeds via multiple reversible steps, including the activation of adenosine 5'phosposulfate (APS) and reduction to sulfite (SO_3^{2}). The kinetic isotope effect (KIE) associated with MSR produces ^{34}S-depleted sulfide and ^{34}S-enriched residual sulfate. Concerning oxygen, the KIE associated with MSR is small, and the equilibrium isotope exchange (EIE) between sulfate and water is kinetically inhibited. However, intermediate sulfur species such as sulfite readily exchange oxygen isotopes with water and become relatively ^{18}O-enriched. Intracellular re-oxidation of this sulfite produces ^{18}O-enriched sulfate. The $\delta^{18}O_{SO4}$-$\delta^{34}S_{SO4}$ trends in residual sulfate are controlled by the expression of the EIE associated with sulfite-water exchange relative to the sulfate reduction rate (SRR). This expression becomes more pronounced when the SRR is lower, or when anaerobic oxidation of methane (AOM) occurs under methane (CH_4) limited conditions, resulting in a steeper slope. After Wortmann et al. (2007), Antler et al. (2013, 2014, 2015), Han et al. (2025).

2 Methods

2.1 Materials and sampling

The sampled barite-bearing fractures are from Proterozoic crystalline bedrock at Forsmark and Laxemar/ Äspö (Southeastern Sweden) (see Drake et al. (2018) for details on the geological setting). Laxemar is situated a couple of kilometers from the

Baltic Sea coastline, and Äspö is an island on the coastline, and here we have merged them into one site (i.e., Laxemar/Äspö) because of their proximity. Drill cores were mainly obtained by triple-tube drilling conducted by the Swedish Nuclear Fuel and Waste Management Co. This drilling technique preserves fragile minerals on fracture surfaces, facilitating the investigation of ancient biological activity in deep fracture systems. Barite was sampled from fractures in a total of 40 drill cores. The samples represented depths ranging from 60 to 1,660 m below sea level. Sample characterization and mineral identification were performed directly on the fracture surfaces using a FEI QUANTA FEG 650 Scanning Electron Microscope (SEM) equipped with an integrated energy dispersive spectroscopy (EDS, Oxford T-Max 80 detector) under low-vacuum conditions. The acceleration voltage was 20 kV, and the instrument was calibrated with a cobalt standard. The barite grains were then hand-picked from the fracture surface under a microscope, included in several epoxy mounts (2.5 cm diameter), and polished to expose the cross-sections of the grains. The polished grains were examined using SEM prior to SIMS analysis to detect growth zonation and avoid impurities and cracks.

2.2 Secondary-ion mass spectrometry (SIMS) analysis of barite (δ^{18}O and δ^{34}S)

Secondary-ion mass spectrometry (SIMS) was conducted on a CAMECA IMS1280 ion probe at the NordSIMS lab, Swedish Museum of Natural History, Stockholm. The analytical routines for sulfur (n = 354) and oxygen (n = 221) isotope analyses of barite follow those described by Drake et al. (2024), which are based on the approaches by Whitehouse (2013) for sulfur and Heinonen et al. (2015) for oxygen. The samples were sputtered using a $^{133}Cs^{+}$ primary beam with 20 kV incident energy and a beam current of ~3 nA, which was rastered over a 5 × 5 µm area during analysis. Each analysis comprised 40 s pre-sputter to remove the gold coating over a 15 × 15 µm area, centering of the secondary beam in the field aperture, and data acquisition in 12 four-second integration cycles. Secondary ion signals (^{32}S and ^{34}S or ^{16}O and ^{18}O) were detected simultaneously using two Faraday detectors with a common mass resolution of 4,860 (M/ΔM) for sulfur and 2,430 (M/ΔM) for oxygen. Data were normalized for instrumental mass fractionation using the S0327 reference material, with a conventionally determined δ^{34}S value of +22.0±0.3 ‰ and δ^{18}O value of +11.0±0.1 ‰ (Liseroudi et al., 2021). All results are reported as $\delta^{34}S_{V\text{-}CDT}$ (Ding et al., 2001) for sulfur and $\delta^{18}O_{V\text{-}SMOW}$ (Coplen, 1995) for oxygen. The typical uncertainties after propagating the within-run and external uncertainties from the standard measurements were ±0.2 ‰ (1σ) for δ^{34}S and between ±0.2 and ±0.6 ‰ (1σ) for δ^{18}O values. The previously published calcite $\delta^{18}O_{V\text{-}PDB}$ values were recalculated to $\delta^{18}O_{V\text{-}SMOW}$ for comparability with barite using the formula $\delta^{18}O_{V\text{-}SMOW} = 1.03092 \times \delta^{18}O_{V\text{-}PDB} + 30.92$. All SIMS data, including previously published data, are compiled in the Supplementary Dataset.

2.3 Cluster analysis

Cluster analysis of the barite δ^{18}O and δ^{34}S data was performed using a Gaussian Mixture Model (GMM) via the Python module Scikit-learn (Pedregosa et al., 2011). The optimal number of components for the GMM was calculated to be three using the Bayesian Information Criterion (BIC). However, the three components yielded regression lines with negative

https://doi.org/10.5194/egusphere-2026-2220
Preprint. Discussion started: 23 April 2026

slopes for the resulting clusters, which is inconsistent with naturally occurring fractionation trends in the $\delta^{18}O$–$\delta^{34}S$ space. Thus, we chose to perform GMM with two components, consistent with the qualitative assumption that sulfate reduction in our system is dominated by two end-member processes (i.e., organoclastic sulfate reduction and anaerobic oxidation of methane). Random state optimization was performed over a range of zero to ten, yielding zero at the minimum BIC. Main axis regression was used to calculate the slopes and R^2 values for the resulting clusters.

3 Results and discussion

We investigated samples from Forsmark and Laxemar exhibiting a $\delta^{34}S_{pyrite}$ range of −53.9 to +131.7 ‰ (Drake et al., 2018) (Table 1, Figs. 2-3). This range was interpreted to reflect Rayleigh distillation during microbial sulfate reduction (MSR) in semi-closed fracture systems, producing ^{34}S-depleted sulfide and extremely ^{34}S-enriched sulfate (Drake et al., 2018). To investigate the record of these microbial processes in ancient barite [$BaSO_4$], we compiled previously published microscale $\delta^{34}S_{pyrite}$, $\delta^{18}O_{calcite}$, and $\delta^{13}C_{calcite}$ data from Drake et al. (2017, 2018) with new SIMS $\delta^{18}O_{barite}$ and $\delta^{34}S_{barite}$ and analyses from Forsmark and Laxemar (Table 1, Figs. 2-3).

Table 1: Stable isotope data ($\delta^{34}S$, $\delta^{18}O$, $\delta^{13}C$) of fracture-hosted minerals (calcite, pyrite, barite) from Forsmark and Laxemar (Fennoscandian Shield, Sweden). Calcite and pyrite data were obtained from Drake et al. (2017, 2018). Barite data were analyzed in this study.

	$\delta^{34}S_{barite}$ (‰, V-CDT)	$\delta^{18}O_{barite}$ (‰, V-SMOW)	$\delta^{34}S_{pyrite}$ (‰, V-CDT)	$\delta^{13}C_{calcite}$ (‰, V-PDB)	$\delta^{18}O_{calcite}$ (‰, V-SMOW)
Forsmark					
n	21	22	793	585	603
Min	+17.2	−0.9	−42.4	−70.3	13.4
Max	+36.8	+16.9	+65.8	+36.5	28.1
Average	+29.7	+12.4	+13.8	−10.8	18.8
Median	+34.5	+15.1	+13.2	−11.8	18.8
1σ	6.5	5.0	16.5	2.4	2.5
Laxemar					
n	323	209	728	352	259
Min	+7.6	+3.1	−53.9	−93.1	10.5
Max	+52.0	+19.7	+131.7	+7.1	28.1
Average	+19.5	+12.3	+32.3	−16.5	20.3
Median	+18.3	+12.3	+23.3	−9.6	21.0
1σ	6.7	3.0	43.8	19.7	3.4

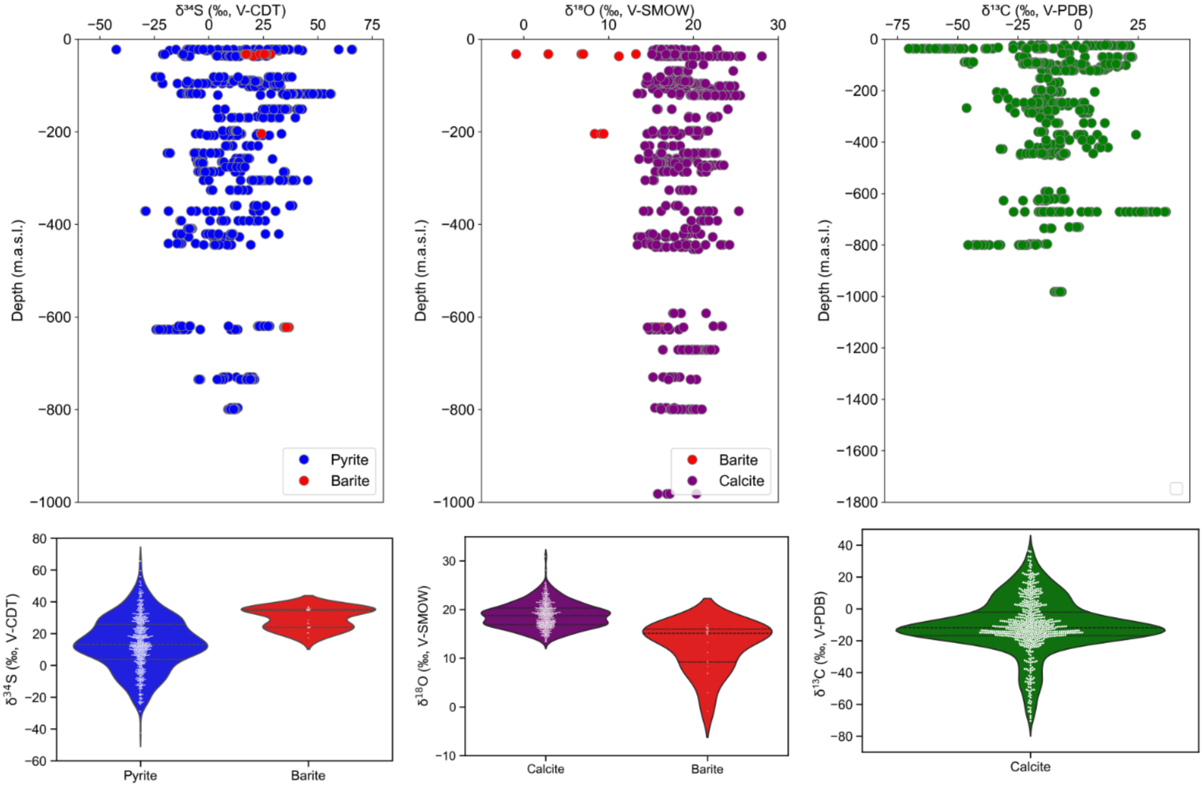

165 **Figure 2: Depth distribution and violin plots of stable isotope data ($\delta^{34}S_{barite}$, $\delta^{34}S_{pyrite}$, $\delta^{18}O_{barite}$, $\delta^{18}O_{calcite}$, and $\delta^{13}C_{calcite}$) for fracture-hosted minerals from Forsmark. Each spot represents one SIMS measurement (m.a.s.l. = meters above sea level). Calcite, pyrite, and barite data were obtained from Drake et al. (2017, 2018) and this study, respectively. $\delta^{18}O_{calcite}$ data were converted from V-PDB to V-SMOW for comparison with $\delta^{18}O_{barite}$.**

https://doi.org/10.5194/egusphere-2026-2220
Preprint. Discussion started: 23 April 2026

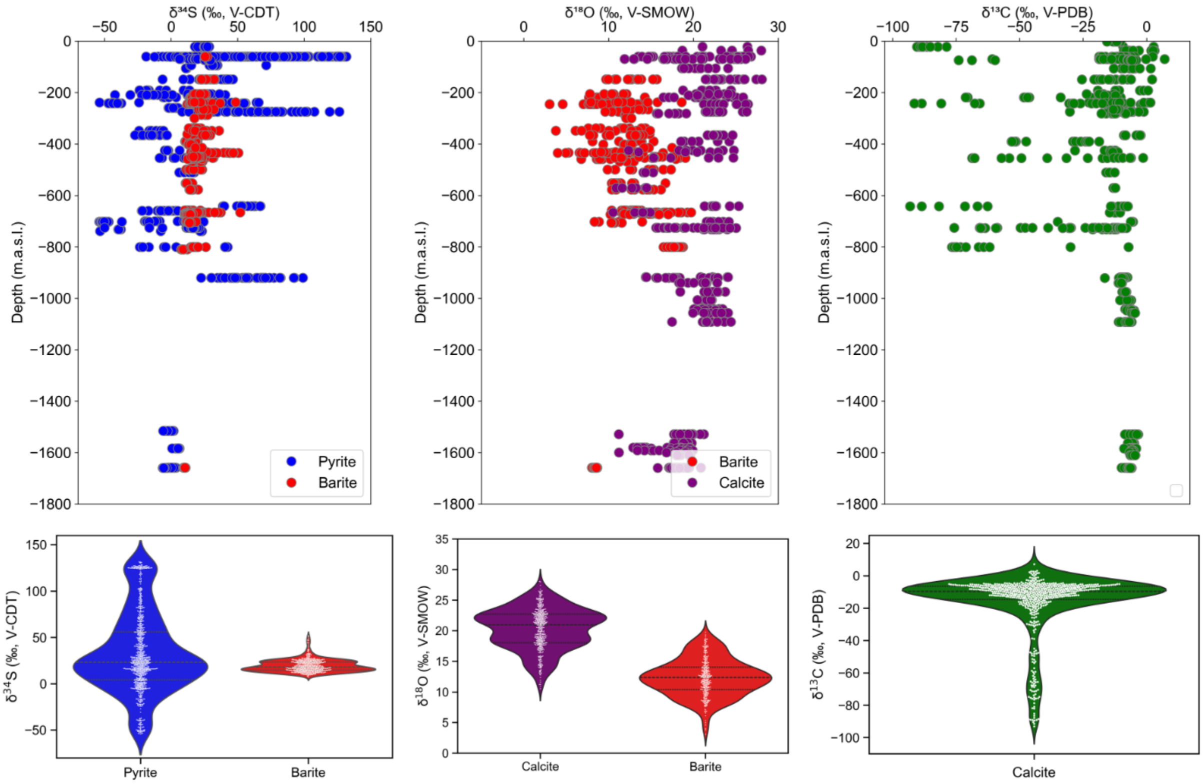

Figure 3: Depth distribution and violin plots of stable isotope data ($\delta^{34}S_{barite}$, $\delta^{34}S_{pyrite}$, $\delta^{18}O_{barite}$, $\delta^{18}O_{calcite}$, and $\delta^{13}C_{calcite}$) of fracture-hosted minerals from Laxemar. Each spot represents one SIMS measurement (m.a.s.l. = meters above sea level). Calcite, pyrite, and barite data were obtained from Drake et al. (2017, 2018) and this study, respectively. $\delta^{18}O_{calcite}$ data were converted from V-PDB to V-SMOW for comparison with $\delta^{18}O_{barite}$.

3.1 Absence of extremely ^{34}S-enriched barite

In Forsmark, $\delta^{34}S_{barite}$ ranged from +17.2 to +36.8 ‰ (median = +34.5 ‰; n = 21), and $\delta^{18}O_{barite}$ ranged from −0.9 to +16.9 ‰ (median = +15.1‰; n = 22). The reconstruction of sulfur sources for barite formation in Forsmark is challenging because of the low number of analyses performed. In Laxemar, $\delta^{34}S_{barite}$ ranged from +7.6 to +52.0 ‰ (median = +18.3 ‰; n = 323), and $\delta^{18}O_{barite}$ ranged from +3.1 to +19.7 ‰ (median = +12.3 ‰; n = 209). The median $\delta^{34}S_{barite}$ (+18.3 ‰) and $\delta^{34}S_{pyrite}$ (+23.3 ‰) values were comparable (Table 1). The $\delta^{34}S_{SO4}$ of the paleo fracture fluids is unknown and likely changed over time. However, assuming a $\delta^{34}S_{SO4}$ similar to the current fracture fluids (+14 to +27 ‰: Drake et al., 2013), dissolved sulfate in such fluids is a plausible sulfur source for barite and pyrite. The total range of $\delta^{34}S_{barite}$ (+7.6 to +52.0 ‰) is much narrower than that of $\delta^{34}S_{pyrite}$ (−53.9 to +131.7 ‰) across Forsmark and Laxemar (Table 1, Figs. 2-3). This was also observed in recently precipitated barite on drill core equipment within a deep borehole at Äspö (Fichtner et al., 2024). Unfortunately, the samples recording the largest ^{34}S-enrichment in our dataset do not have co-genetic $\delta^{34}S_{pyrite}$ data due to absence of pyrite, making it difficult to establish the relationship between barite and pyrite. Regardless, neither modern nor ancient subsurface barite from Forsmark or Laxemar records the extreme ^{34}S-enrichment predicted by $\delta^{34}S_{pyrite}$ data.

3.2 Microbial sulfur cycling recorded in ancient barite

The co-variation of the $\delta^{18}O_{barite}$ and $\delta^{34}S_{barite}$ values in our dataset follows two distinct trends (Fig. 4a). We applied a Gaussian Mixture Model (GMM) to discriminate our $\delta^{18}O_{barite}$ and $\delta^{34}S_{barite}$ data into two groups (Fig. 4b), which are hereafter referred to as 'Group 1' and 'Group 2'. Major axis regression yielded slopes of 0.93 (R^2= 0.49) and 0.48 (R^2=0.80) for the Group 1 and Group 2 trends, respectively (Fig. 4b). The poor R^2 values can be explained by the origin of the data points from different localities and barite growth generations. Thus, each of the two groups reflects multiple fractionation processes occurring in separate fractures and at different times. There was no correlation between Group 1 and Group 2 barite and the $\delta^{18}O$ values of co-genetic calcite (Fig. 4c). This suggests that the trends observed in barite do not correspond to different environments with specific hydrogeochemical regimes (Pedersen et al., 1997). Instead, they most likely record different processes affecting the respective sulfate reservoirs during barite formation.

Ancient microbial sulfur cycling in deep subsurface fractures at Forsmark and Laxemar was demonstrated by coupled $\delta^{34}S_{pyrite}$ and $\delta^{13}C_{calcite}$ signatures of organoclastic sulfate reduction (OSR) and sulfate-dependent anaerobic oxidation of methane (AOM) (Drake et al., 2013, 2015a, 2018, 2021). A prominent role of thermochemical sulfate reduction (TSR) in these localities has been ruled out because of the large degree of fractionation between plausible $\delta^{34}S_{SO4}$ values of fracture fluids in these systems and pyrite ($^{34}\varepsilon = \delta^{34}S_{SO4}-\delta^{34}S_{pyrite}$= 55 to 66 ‰; Drake et al., 2021). Moreover, fluid inclusion data indicating homogenization temperatures of coeval calcite (<100 °C: Drake et al., 2018), and clumped isotope derived temperatures of 51±5 to 98±10 °C of the calcite (Herlambang et al., 2023) do not support TSR, which generally occurs at temperatures >100 °C (Machel, 2001). The overall ranges of $\delta^{18}O_{barite}$ (−0.9 to +19.7 ‰) and $\delta^{34}S_{barite}$ (+7.6 to +52.0 ‰) across both localities are consistent with MSR, which can produce ^{18}O- and ^{34}S-enrichment in the residual sulfate pool (Antler et al., 2013, 2014, 2015; Brunner et al., 2005; Drake et al., 2018; Jørgensen et al., 2004; Paiste et al., 2022; Rudnicki et al., 2001; Wortmann et al., 2007; Zaback et al., 1993). These observations strongly suggest a record of MSR in co-genetic barite from both localities.

To distinguish biosignatures of OSR and AOM recorded in barite, we correlated our $\delta^{18}O_{barite}$ and $\delta^{34}S_{barite}$ data with the $\delta^{13}C$ values of co-genetic calcite generations (Fig. 4d). When petrographic correlation of barite with calcite generations was not possible, we used the average $\delta^{13}C_{calcite}$ values from the barite-bearing samples. Strongly ^{13}C-depleted calcite ($\delta^{13}C \approx -70$ to −40 ‰) was almost exclusively associated with Group 1 barite (Fig. 4d). Such strong ^{13}C-depletion as −70‰ suggests anaerobic oxidation of primarily microbial methane with limited input from other carbon sources (Drake et al., 2015a, 2017). However, Group 1 also contains barite associated with less ^{13}C-depleted calcite ($\delta^{13}C \approx -40$ to −10 ‰), which generally is inconsistent with methane as the main carbon source (Whiticar, 1999). Instead, this calcite may have been derived from the heterotrophic oxidation of organic carbon (Schidlowski, 2001), implying an association with OSR. Group 2 barite is almost exclusively associated with calcite that has a $\delta^{13}C \approx -20$ ‰ or higher (Fig. 4d), implying a dominant role of OSR (Drake et al., 2017). Thus, the formation of Group 1 barite may have been affected by both AOM and OSR, whereas the formation of Group 2 barite was predominantly affected by OSR.

https://doi.org/10.5194/egusphere-2026-2220
Preprint. Discussion started: 23 April 2026

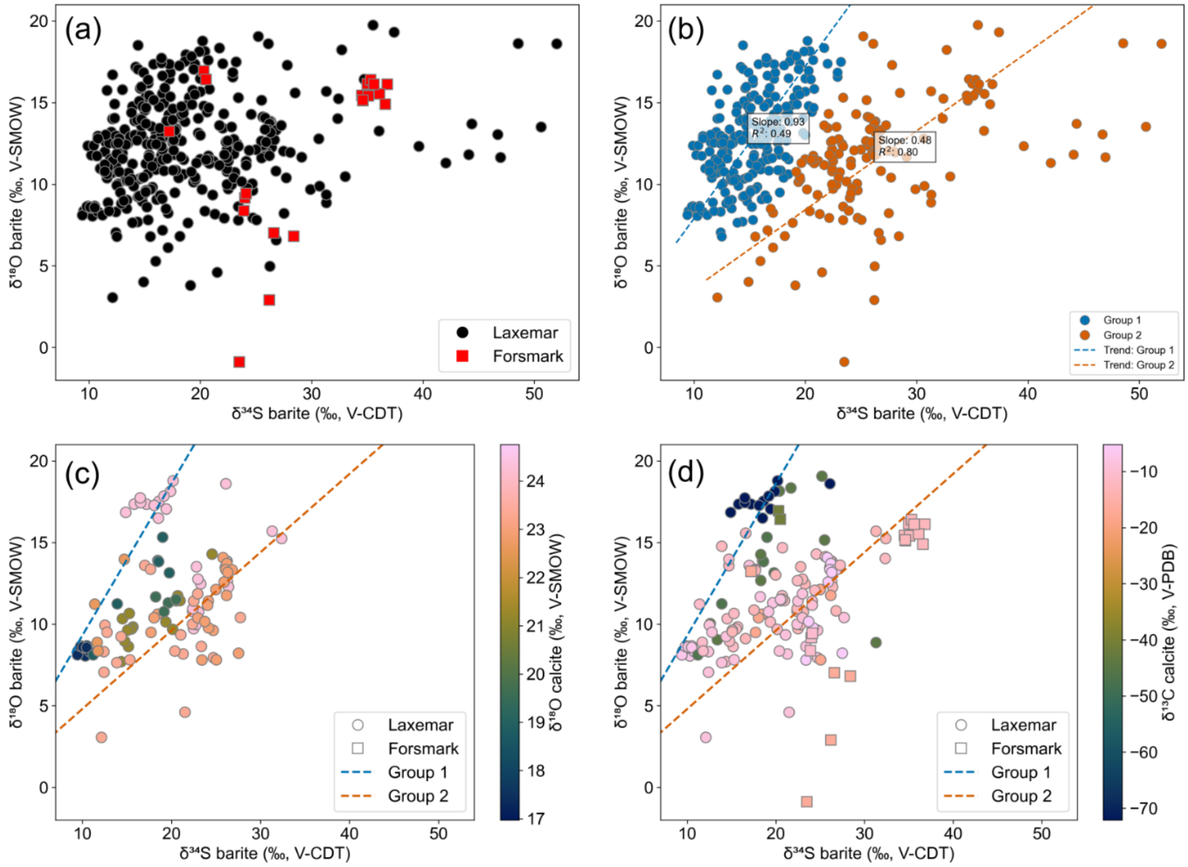

Figure 4: Stable isotope cross plots and Gaussian Mixture Model (GMM) of barite δ^{18}O and δ^{34}S data vs. calcite δ^{18}O and δ^{13}C data. Each spot represents one SIMS analysis. (a) δ^{18}O and δ^{34}S analyses of barite. (b) GMM of barite δ^{18}O and δ^{34}S data using two cluster centers, yielding 'Group 1' barite and 'Group 2' barite. Major axis regression of both groups revealed slopes of 0.93 and 0.48, respectively. (c) δ^{18}O and δ^{34}S analyses of barite color-coded by δ^{18}O of calcite in the same sample. There was no apparent correlation between the Group 1 and Group 2 trends and their corresponding $\delta^{18}O_{calcite}$ values, demonstrating that the trends arise from fractionation processes affecting the sulfate reservoir, rather than fluid mixing. Note that there were no samples from Forsmark with coupled $\delta^{18}O_{barite}$-$\delta^{34}S_{barite}$-$\delta^{13}C_{calcite}$ data. (d) δ^{18}O and δ^{34}S analyses of barite color-coded by $\delta^{13}C_{calcite}$ in the same sample. The $\delta^{13}C_{calcite}$ data suggest that AOM barite occurs almost exclusively in Group 1. In contrast, OSR-related barite occurred in Groups 1 and 2. Note that the AOM-related Group 1 barite follows a steeper trend than the OSR-dominated Group 2, contrary to observations by Antler et al. (2014). The color coding in (c) & (d) follows recommendations for scientifically derived color maps (Crameri et al., 2020).

3.3 Controls on δ^{18}O/ δ^{34}S trends in barite: pathways versus rates of microbial sulfate reduction

We found a steeper δ^{18}O/ δ^{34}S trend in the AOM-affected Group 1 than in the OSR-dominated Group 2 (Fig. 4d). A steeper δ^{18}O/ δ^{34}S trend suggests a higher degree of sulfur-intermediate re-oxidation relative to sulfate reduction (Antler et al., 2013; Brunner et al., 2005; Wortmann et al., 2007). The relationship between sulfur-intermediate re-oxidation relative to sulfate reduction during the early stages of MSR can be controlled by different metabolic processes (OSR vs. AOM) and sulfate reduction rates (SRR) (Antler et al., 2013; Brunner et al., 2005; Wortmann et al., 2007). The slope of the Group 1 trend

https://doi.org/10.5194/egusphere-2026-2220
Preprint. Discussion started: 23 April 2026

matches previous observations from methane-limited AOM settings (Antler et al., 2015), consistent with our $\delta^{13}C_{calcite}$ evidence for AOM in Group 1 (Fig. 4d). Thus, our combined $\delta^{18}O_{barite}$, $\delta^{34}S_{barite}$, and $\delta^{13}C_{calcite}$ data may record AOM under methane-limited conditions in Group 1. However, several data points in Group 1 did not show evidence of AOM. Additionally, the trend of the OSR-dominated Group 2 is much shallower than OSR-associated trends previously observed in sedimentary environments (Fig. 4d) (Antler et al., 2013, 2014). Thus, the variation of $\delta^{18}O_{barite}$/ $\delta^{34}S_{barite}$ trends at Forsmark and Laxemar is apparently not only controlled by the co-occurrence of different metabolic processes.

The variability of $\delta^{18}O$/ $\delta^{34}S$ trends in OSR-associated barite may thus be interpreted as a lower SRR in Group 1 than in Group 2 (Fig. 4). Notably, the largest ^{34}S enrichment occurs in the OSR-dominated Group 2 (+12.1 to +52.0 ‰; median = +25.3 ‰; Table 2, Fig. 4b), implying a large apparent $^{34}\varepsilon$. The major control on SRR and $^{34}\varepsilon$ is the balance between the availability of sulfate and electron donors (Bradley et al., 2016; Sim et al., 2023; Wing and Halevy, 2014). If the sulfate supply is low relative to that of electron donors, sulfate consumption is rapid and quantitative, while $^{34}\varepsilon$ is diminished. In contrast, if the sulfate supply is high and the electron donor supply is limited, SRR is low, and $^{34}\varepsilon$ is high. Hence, variations in SRR observed in relatively sulfate-rich marine sediments (28 mM in seawater: Jørgensen et al., 2019) are generally controlled by the availability of organic substrates (Leavitt et al., 2013). However, the typical range of sulfate concentrations in modern anoxic fracture fluids at Forsmark and Laxemar is 1-10 mM (Hallbeck & Pedersen, 2008; Laaksoharju et al., 2008; Drake et al., 2013), implying a more rate-limiting function for sulfate availability in the deep subsurface.

Relatively low sulfate availability in Group 1 is supported by associated $\delta^{13}C$ evidence for AOM (Fig. 4d). In aquatic systems, AOM is favored at the sulfate-methane transition zone (SMTZ) where upward-diffusing methane produced by methanogens meets downward-diffusing sulfate (Egger et al., 2018; Knittel and Boetius, 2009; Reeburgh, 2007). Thus, the evidence for AOM in Group 1 requires both a methane and a sulfate source for the fracture environment. Substantial methanogenesis is typically only observed below and within the (SMTZ) (Iversen & Jorgensen, 1985; Glossner et al., 2016; Sela-Adler et al., 2017). This is because sulfate reducers generally outcompete methanogens for substrate utilization above sulfate concentrations of (~1-10 mM) (Iversen & Jorgensen, 1985; Glossner et al., 2016; Sela-Adler et al., 2017). Therefore, if sulfate concentrations exceed this threshold, methanogenesis and AOM may be inhibited. Instead, sulfate reduction may then dominantly proceed via OSR. Thus, a lower sulfate availability may plausibly explain both the evidence for AOM and a lower SRR in Group 1, whereas a higher sulfate availability may explain the predominance of OSR and higher SRR in Group 2.

Notably, the trend of our OSR-associated Group 2 is shallower than previously observed OSR-related sulfate in marine environments (Antler et al., 2013, 2014). It seems unlikely that this can be explained by higher SRR than in marine sediments. The deep continental subsurface is a dominantly oligotrophic environment (Hoehler and Jørgensen, 2013), suggesting a generally low availability of electron donors for sulfate reduction. Indeed, current fracture fluids at Forsmark and Laxemar/Äspö show low dissolved organic carbon contents (<0.2 mM: Drake et al., 2013). This organic carbon is also highly refractory, limiting its bioavailability (Osterholz et al., 2022). For these reasons, SRR are generally lower than in marine sediments, predicting a steeper trend in the subsurface, opposite to our observation. However, sulfur isotope analyses have repeatedly shown relatively large apparent $^{34}\varepsilon$ values in the deep biosphere (Drake et al., 2015b, 2018; Wortmann et al., 2001). Thus, large OSR-associated $^{34}\varepsilon$ values may have caused a stronger ^{34}S-enrichment of the residual sulfate pool at our study site, and thus a faster increase of $\delta^{34}S_{SO4}$ relative to $\delta^{18}O_{SO4}$ (i.e., a shallower trend) compared to marine sediments. In summary, we attribute the different trends of Group 1 and 2 to an interplay of different MSR pathways, and variations of SRR and $^{34}\varepsilon$ due to paleoenvironmental sulfate/ electron donor abundance ratios.

Table 2: Statistical parameters of the groups resulting from the Gaussian Mixture Model.

	Min	Max	Median	Average	1σ
Group 1 (n=224)					
$\delta^{34}S_{barite}$ (‰, V-CDT)	+9.4	+23.2	+15.1	+15.2	3.0
$\delta^{18}O_{barite}$ (‰, V-SMOW)	+6.8	+18.8	+12.7	+12.8	2.8
Group 2 (n=142)					
$\delta^{34}S_{barite}$ (‰, V-CDT)	+12.1	+52.0	+25.3	+26.6	7.2
$\delta^{18}O_{barite}$ (‰, V-SMOW)	−0.9	+19.8	+11.8	+11.6	3.5

3.4 Insights from integrating microscale δ^{18}O-δ^{34}S-δ^{13}C records

Microscale observations of barite-pyrite-calcite assemblages support an interplay of MSR pathways and rates in controlling stable isotope records at Forsmark and Laxemar (Figs. 5,6). Barite in sample KAS02 (802 m) can be taken as a prime example, it is intergrown with calcite that has an average δ^{13}C of −72.1 ‰, demonstrating an influence of AOM during barite formation (Figs. 5a,b). This is consistent with the GMM assignment of all SIMS spots on barite in this sample to the AOM-affected Group 1 (Fig. 5c). Notably, this barite exhibited distinct crystallographic zonation with minor core-to-rim δ^{34}S and δ^{18}O increases of ~4 ‰ and ~0.8 ‰, respectively (Fig. 5c-e). This crystallographic and isotopic zonation is consistent with MSR affecting a diminishing sulfate pool during barite growth (Fichtner et al., 2024; Wood et al., 2021). At the same time, pyrite in this sample displays a much more pronounced core-to-rim δ^{34}S increase of ca. 15 to 60 ‰ (Fig. 5f), implying a high degree of Rayleigh distillation during pyrite growth. Thus, Rayleigh distillation during AOM produced ^{34}S-enriched pyrite but no correspondingly heavy barite in this sample. This implies that barite and pyrite formed under different hydrogeochemical conditions, with pyrite likely recording a later stage of the Rayleigh cycle.

Sample KLX01 (220 m) serves as an example for OSR-related barite due to its association with calcite lacking a substantial δ^{13}C depletion (Fig. 6a,b). Notably, barite in this sample exhibited a massive core and a porous rim (Fig. 6c). These texturally distinct growth zones were associated with a sharp core-to-rim δ^{34}S and δ^{18}O increase of ~12 ‰ and ~6 ‰, respectively (Fig. 6c-e). This sharp increase suggests that barite in the rim precipitated from sulfate that had already undergone ^{34}S-enrichment via sulfate reduction elsewhere in the fracture system (e.g., Drake et al., 2018). Thus, the distinct textural and isotopic differences demonstrate that the generations reflect two barite precipitation events, rather than continuous barite growth. Notably, SIMS spots related to Group 1 predominated in the core, whereas spots related to Group 2 exclusively occurred in the rim (Fig. 6c). The porosity in the rim is consistent with barite dissolution due to undersaturation (Fichtner et al., 2024), which may have arisen from the high SRR inferred for Group 2. Relatively minor core-to-rim $\delta^{34}S$ increase of ca. 0 to 20 ‰ in co-genetic pyrite imply that sulfate did not become strongly depleted during pyrite formation in this microenvironment (Fig. 6f). While there was no evidence for AOM from $\delta^{13}C_{calcite}$ in this sample, it cannot be resolved petrographically whether the calcite and pyrite are co-genetic to the barite core or rim. Therefore, it remains unclear whether the shift from Group 1 to Group 2 during barite growth is due to different MSR pathways or SRR. Irrespective of this problem, the differences between KAS02 (802 m) and KLX01 (220 m), as well as their evolution during barite growth, demonstrate a strong control of hydrogeochemical conditions on their isotopic composition in different microenvironments and over time.

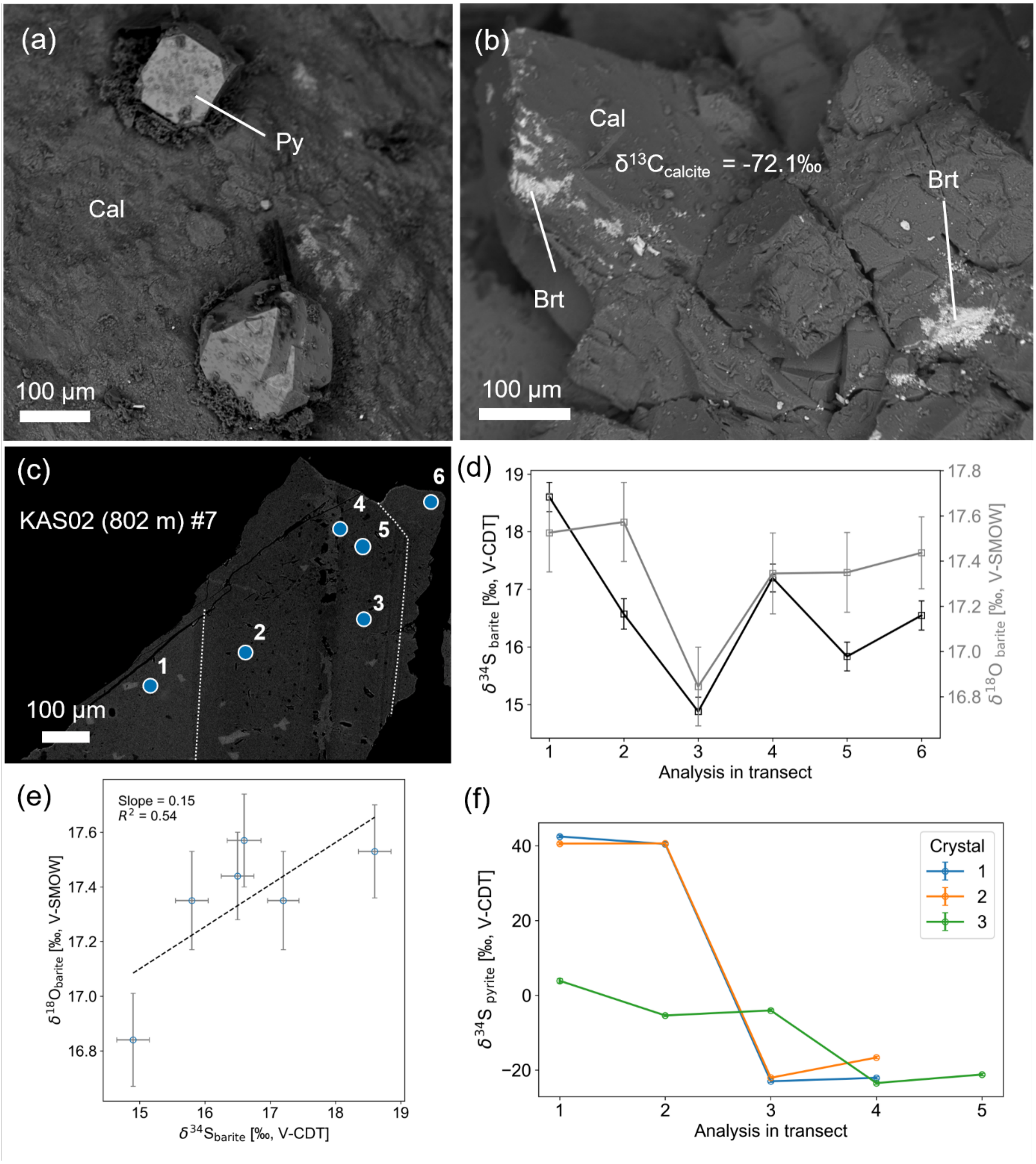

Figure 5: BSE images and stable isotope data of sample KAS02 (802 m depth) from Äspö (i.e., Laxemar). (a) Euhedral pyrite (Py) intergrown with calcite (Cal), demonstrating that pyrite is co-genetic with the outermost calcite generation. (b) Barite (Brt) on the surface of a calcite crystal, demonstrating the coeval formation of barite and calcite. Calcite in this sample has a $\delta^{13}C_{calcite}$ of −72.1‰, demonstrating calcite precipitation after the oxidation of biogenic methane via AOM (Drake et al., 2017). (c) SEM image of polished barite crystal showing growth zonation and $\delta^{34}S_{barite}$ and $\delta^{18}O_{barite}$ SIMS spots. The white dashed line highlights the boundary between crystallographic growth zones. The color coding of the analysis spots signifies their assignment to Group 1

(blue) according to Fig. 3b. (d) Transect across zoned barite crystal in (c) showing co-variation of $\delta^{34}S_{barite}$ and $\delta^{18}O_{barite}$ with higher ^{34}S- and ^{18}O-enriched values in the later generation (rim). (d) $\delta^{34}S_{barite}$ vs $\delta^{18}O_{barite}$ scatter plot showing a slope of 0.15. (f) Transect across three pyrite grains from the same sample (Drake et al., 2018), showing a $\delta^{34}S_{pyrite}$ variation of ca. 65‰ across two of the grains. Error bars in f) are smaller than the symbols.

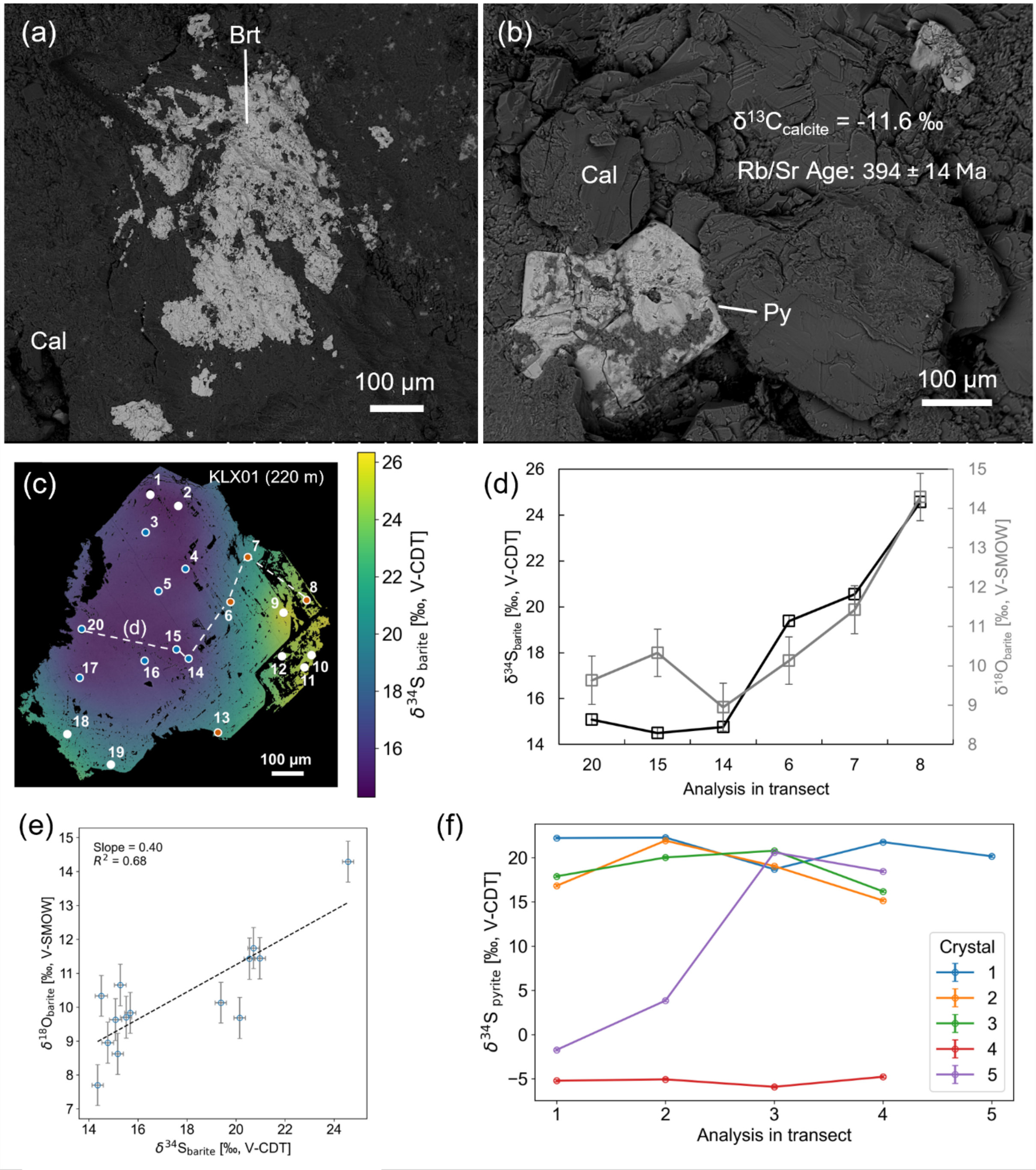

Figure 6: Backscatter electron images and stable isotope data for sample KLX01 (220 m depth) from Laxemar. (a) Barite (Brt) on the surface of calcite (Cal), demonstrating that barite is co-genetic with the outermost calcite generation. (b) Pyrite (Py) intergrown with calcite surface, demonstrating the coeval formation of pyrite with calcite and, thus, barite. The calcite generation coeval with barite shows a Rb/Sr age of 394 ± 14 Ma and $\delta^{13}C_{calcite} = -11.6‰$. (c) heatmap interpolated via cubic convolution of $\delta^{34}S$ values on a polished barite crystal showing two distinct growth zones and $\delta^{34}S_{barite}$ and $\delta^{18}O_{barite}$ SIMS spots. The color coding of the analysis spots signifies their assignment to Group 1 (blue) and Group 2 (orange) according to Fig. 3b. White dots could not be assigned to a group because corresponding $\delta^{18}O_{barite}$ values were lacking. The predominance of Group 1 in the core and Group 2 in the rim suggests an increase in sulfate reduction rate (SRR) during barite growth. The dashed line marks the transect in (d). (d) transect across zoned barite crystal in (c) showing co-variation of $\delta^{34}S_{barite}$ and $\delta^{18}O_{barite}$ with more ^{34}S- and ^{18}O-enriched values in the later generation (Rim). (e) $\delta^{34}S_{barite}$ vs $\delta^{18}O_{barite}$ scatter plot of the barite crystal in c) and d). f) transect across five pyrite grains from the same sample (Drake et al., 2018), showing a $\delta^{34}S_{pyrite}$ variation of ca. 20‰ across one grain. Error bars in f) are smaller than the symbols.

3.5 Implications for biosignature records in deep subsurface barite

We interpreted the stable isotope records in ancient subsurface barite to reflect the interplay between MSR pathways, SRR, and $^{34}\varepsilon$ values, controlled by microenvironmental sulfate/electron donor ratios (Fig. 7). The $\delta^{13}C_{calcite}$ evidence for AOM implies that Group 1 barite formed in a relatively low-sulfate environment. When sulfate availability is limited, methanogenesis and/or AOM is favored, and SSR is low, resulting in a steep trend in Group 1 (Fig. 7a). At higher sulfate availability, methanogenesis is inhibited, possibly resulting in the lack of evidence for AOM in Group 2 (Fig. 7b). Instead, OSR is favored and SRR is high, resulting in a stronger ^{34}S-enrichment and a shallower trend in Group 2 (Fig. 7b). This ^{34}S-enrichment suggests that the SRR at times exceeded the sulfate resupply, decreasing the steady state sulfate concentration (i.e., closed system conditions). This highlights a strong control of local hydrogeochemical conditions on biosignature records in ancient barite from deep fracture systems.

Variations in the SRR may explain why barite does not record the sulfate reservoir present during the precipitation of extremely ^{34}S-enriched pyrite in the deep subsurface. At a lower SRR (Group 1), $\delta^{18}O_{SO4}$ rises rapidly relative to $\delta^{34}S_{SO4}$, whereas at a higher SRR (Group 2), $\delta^{18}O_{SO4}$ rises slowly relative to $\delta^{34}S_{SO4}$ (Fig. 4). The observed ^{34}S-enrichment in Group 2 ($\delta^{34}S_{barite} \leq 52.0$ ‰) shows that Rayleigh distillation can be recorded in subsurface barite, although not to the extreme degree observed in pyrite elsewhere in the system (Fig. 4). Extreme ^{34}S-enrichments are not recorded because barite undersaturation is reached when the sulfate pool is depleted to the point where $\delta^{34}S_{SO4} = +52.0$ ‰, which is the maximum recorded value in barite (Fig. 4, Table 1) (cf. Fichtner et al., 2024). This is consistent with textural evidence for barite dissolution in the Group-2-related rim of sample KLX01 (220 m) (Fig. 6c). Thus, we suggest a preservation bias against extremely ^{34}S-enriched barite at high degrees of Rayleigh distillation explains its absence in deep subsurface environments.

The absence of strong ^{34}S-enrichment in AOM-related barite from Group 1 implies that the record of closed-system Rayleigh distillation in subsurface barite is restricted to OSR-related processes, consistent with observations from pyrite (Drake et al., 2018). This contrasts with observations from marine sediments, where ^{34}S-enriched barite is a commonly used proxy for AOM at the SMTZ (Torres et al., 1996; Wood et al., 2021; Yang et al., 2023; Zan et al., 2022; Zhou et al., 2015). This discrepancy is possibly due to the higher sulfate concentration in seawater, allowing sulfate to become strongly ^{34}S-enriched before barite becomes undersaturated (Fichtner et al., 2024). This highlights that interpretation frameworks for stable isotope signatures in marine barite cannot be directly applied to deep subsurface barite.

The presence of biosignatures for OSR and AOM at Forsmark and Laxemar demonstrates that ancient barite from deep subsurface environments can record diverse pathways of microbial sulfur cycling. The Rb/Sr age of calcite coeval with OSR-related barite in sample KLX01 (220 m) was dated to 394±14 Ma (Fig. 6b) (Drake et al., 2017). This shows that barite has recorded signatures of deep microbial sulfur cycling in the Fennoscandian Shield since the Devonian. Signatures of metabolic processes in barite varied over time within the same microenvironment and between different fractures. Understanding deep subsurface geobiology thus requires microscale analyses distributed over large crustal volumes. Moreover, distinguishing OSR and AOM was aided by tying $\delta^{13}C_{calcite}$ values with trajectories in $\delta^{18}O_{barite}$/ $\delta^{34}S_{barite}$ space. Thus, our study highlights the need for microscale multiple stable isotope analyses of co-genetic mineral assemblages.

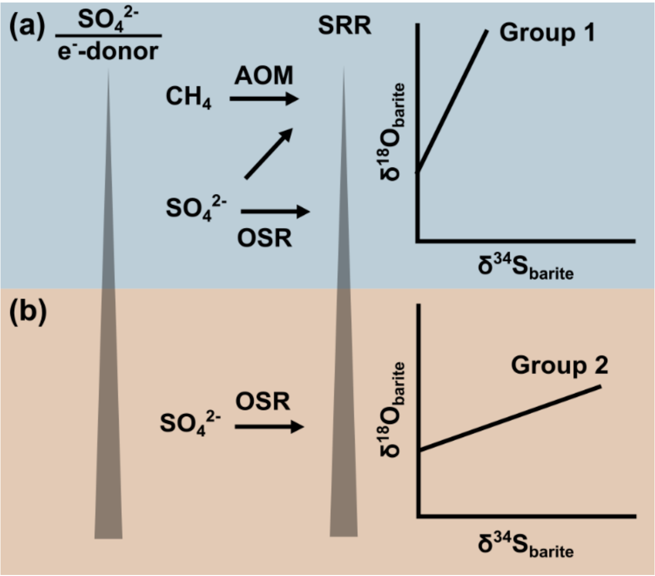

Figure 7: Conceptual model of the controls on $\delta^{18}O_{barite}$ and $\delta^{34}S_{barite}$ systematics in the continental deep subsurface. (a) at a lower sulfate/ electron donor ratio, microbial methanogenesis is active. Microbial sulfate reduction (MSR) proceeds via both sulfate-dependent anaerobic oxidation of methane (AOM) and organoclastic sulfate reduction (OSR), at a relatively low sulfate reduction rate (SRR). This results in the steep $\delta^{18}O_{barite}$/ $\delta^{34}S_{barite}$ trend recorded in Group 1 barite. (b) at a higher sulfate/ electron donor ratio, microbial methanogenesis is inhibited, and MSR proceeds predominantly via OSR at relatively high SRR. This results in the shallow $\delta^{18}O_{barite}$/ $\delta^{34}S_{barite}$ trend recorded in Group 2.

4 Conclusions

We compiled previously published microscale $\delta^{34}S_{pyrite}$ and $\delta^{18}O_{calcite}$ and $\delta^{13}C_{calcite}$ data with new SIMS $\delta^{34}S_{barite}$ and $\delta^{18}O_{barite}$ analyses to investigate biosignature records in ancient deep subsurface mineral assemblages from Forsmark and Laxemar/ Äspö (Southeastern Sweden). We identified two groups of barite recording microbial sulfate reduction (MSR) associated with distinct $\delta^{18}O$/ $\delta^{34}S$ trends. Comparison with coeval $\delta^{13}C_{calcite}$ data revealed that Group 1 was dominated by sulfate-dependent anaerobic oxidation of methane (AOM), whereas Group 2 was dominated by organoclastic sulfate reduction

(OSR). The different trends likely resulted from an interplay of different MSR pathways (AOM vs. OSR), as well as variations of sulfate reduction rates (SRR) and $^{34}\varepsilon$. We attribute these variations to paleoenvironmental sulfate/ electron donor abundance ratios: lower ratios favored methanogenesis and AOM at lower SRR, whereas higher ratios inhibited methanogenesis and favored OSR at higher SRR. Strong ^{34}S-enrichment was only detected in Group 2 (up to $\delta^{34}S_{barite}$ = +52.0 ‰), although not to the extreme degree observed in some pyrite from the same locality ($\delta^{34}S_{pyrite}$ = +131.7 ‰). We suggest a preservation bias against extremely ^{34}S-enriched barite due to undersaturation at high degrees of Rayleigh distillation explains its absence in deep subsurface environments. Our study highlights that multiple stable isotope signatures in fracture-hosted mineral assemblages provide insights into metabolic processes in the ancient deep biosphere, but these records are strongly affected by local hydrogeochemical conditions.

Data availability

All data presented in the manuscript are available in the Supplementary Dataset.

Author contributions

ER: Data curation, Formal analysis, Investigation, Methodology, Validation, Visualization, Writing (original draft preparation), Writing (review and editing). VF: Data curation, Investigation, Formal analysis, Writing (review and editing). MT: Data curation, Investigation, Formal analysis, Writing (review and editing). MW: Resources, Writing (review and editing). HD: Conceptualization, Funding acquisition, Methodology, Project administration, Resources, Supervision, Writing (review and editing).

Competing interests

The authors declare no competing interests.

Acknowledgements

This work was supported by grants of the Swedish Nuclear Fuel and Waste Management Co. (SKB), Swedish research council (2021-04365, 2025-04466), Formas (2020-01577), J. Gust. Richert foundation (2023-00850), the Crafoord foundation (20210524), and National Science Foundation (2120733) to Henrik Drake. We thank Heejin Jeon for assistance in SIMS sample preparation and analysis. This is NordSIMS publication #XXX.

References

Aloisi, G., Bouloubassi, I., Heijs, S. K., Pancost, R. D., Pierre, C., Sinninghe Damsté, J. S., Gottschal, J. C., Forney, L. J., and Rouchy, J.-M.: CH4 -consuming microorganisms and the formation of carbonate crusts at cold seeps, Earth and Planetary Science Letters, 203, 195–203, https://doi.org/10.1016/S0012-821X(02)00878-6, 2002.

Antler, G., Turchyn, A. V., Rennie, V., Herut, B., and Sivan, O.: Coupled sulfur and oxygen isotope insight into bacterial sulfate reduction in the natural environment, Geochimica et Cosmochimica Acta, 118, 98–117, https://doi.org/10.1016/j.gca.2013.05.005, 2013.

Antler, G., Turchyn, A. V., Herut, B., Davies, A., Rennie, V. C. F., and Sivan, O.: Sulfur and oxygen isotope tracing of sulfate driven anaerobic methane oxidation in estuarine sediments, Estuarine, Coastal and Shelf Science, 142, 4–11, https://doi.org/10.1016/j.ecss.2014.03.001, 2014.

Antler, G., Turchyn, A. V., Herut, B., and Sivan, O.: A unique isotopic fingerprint of sulfate-driven anaerobic oxidation of methane, Geology, 43, 619–622, https://doi.org/10.1130/G36688.1, 2015.

Bar-On, Y. M., Phillips, R., and Milo, R.: The biomass distribution on Earth, Proc. Natl. Acad. Sci. U.S.A., 115, 6506–6511, https://doi.org/10.1073/pnas.1711842115, 2018.

Bell, E., Lamminmäki, T., Alneberg, J., Qian, C., Xiong, W., Hettich, R. L., Frutschi, M., and Bernier-Latmani, R.: Active anaerobic methane oxidation and sulfur disproportionation in the deep terrestrial subsurface, The ISME Journal, 16, 1583–1593, https://doi.org/10.1038/s41396-022-01207-w, 2022.

Böttcher, M. E., Bernasconi, S. M., and Brumsack, H.-J.: 32. Carbon, sulfur, and oxygen isotope geochemistry of interstitial waters from the Western Mediterranean, in: Proceedings of the Ocean Drilling Program, 161 Scientific Results, vol. 161, edited by: Zahn, R., Comas, M. C., and Klaus, A., Ocean Drilling Program, https://doi.org/10.2973/odp.proc.sr.161.1999, 1999.

Boudreau, B. P. and Westrich, J. T.: The dependence of bacterial sulfate reduction on sulfate concentration in marine sediments, Geochimica et Cosmochimica Acta, 48, 2503–2516, https://doi.org/10.1016/0016-7037(84)90301-6, 1984.

Bradley, A. S., Leavitt, W. D., Schmidt, M., Knoll, A. H., Girguis, P. R., and Johnston, D. T.: Patterns of sulfur isotope fractionation during microbial sulfate reduction, Geobiology, 14, 91–101, 2016.

Brunner, B., Bernasconi, S. M., Kleikemper, J., and Schroth, M. H.: A model for oxygen and sulfur isotope fractionation in sulfate during bacterial sulfate reduction processes, Geochimica et Cosmochimica Acta, 69, 4773–4785, https://doi.org/10.1016/j.gca.2005.04.017, 2005.

Campbell, K. A., Farmer, J. D., and Des Marais, D.: Ancient hydrocarbon seeps from the Mesozoic convergent margin of California: carbonate geochemistry, fluids and palaeoenvironments, Geofluids, 2, 63–94, https://doi.org/10.1046/j.1468-8123.2002.00022.x, 2002.

Chambers, L. A., Trudinger, P. A., Smith, J. W., and Burns, M. S.: Fractionation of sulfur isotopes by continuous cultures of Desulfovibrio desulfuricans, Canadian Journal of Microbiology, 21, 1602–1607, 1975.

Chivian, D., Brodie, E. L., Alm, E. J., Culley, D. E., Dehal, P. S., DeSantis, T. Z., Gihring, T. M., Lapidus, A., Lin, L.-H., Lowry, S. R., Moser, D. P., Richardson, P. M., Southam, G., Wanger, G., Pratt, L. M., Andersen, G. L., Hazen, T. C., Brockman, F. J., Arkin, A. P., and Onstott, T. C.: Environmental Genomics Reveals a Single-Species Ecosystem Deep Within Earth, Science, 322, 275–278, https://doi.org/10.1126/science.1155495, 2008.

Coplen, T. B.: Discontinuance of SMOW and PDB, Nature, 375, 285, 1995.

Crameri, F., Shephard, G. E., and Heron, P. J.: The misuse of colour in science communication, Nat Commun, 11, https://doi.org/10.1038/s41467-020-19160-7, 2020.

Crockford, P. W., Kunzmann, M., Bekker, A., Hayles, J., Bao, H., Halverson, G. P., Peng, Y., Bui, T. H., Cox, G. M., Gibson, T. M., Wörndle, S., Rainbird, R., Lepland, A., Swanson-Hysell, N. L., Master, S., Sreenivas, B., Kuznetsov, A., Krupenik, V., and Wing, B. A.: Claypool continued: Extending the isotopic record of sedimentary sulfate, Chemical Geology, 513, 200–225, https://doi.org/10.1016/j.chemgeo.2019.02.030, 2019.

Ding, T., Valkiers, S., Kipphardt, H., De Bièvre, P., Taylor, P. D. P., Gonfiantini, R., and Krouse, R.: Calibrated sulfur isotope abundance ratios of three IAEA sulfur isotope reference materials and V-CDT with a reassessment of the atomic weight of sulfur, Geochimica et Cosmochimica Acta, 65, 2433–2437, https://doi.org/10.1016/S0016-7037(01)00611-1, 2001.

Drake, H. and Reiners, P. W.: Thermochronologic perspectives on the deep-time evolution of the deep biosphere, Proc. Natl. Acad. Sci. U.S.A., 118, e2109609118, https://doi.org/10.1073/pnas.2109609118, 2021.

Drake, H., Åström, M. E., Tullborg, E.-L., Whitehouse, M., and Fallick, A. E.: Variability of sulphur isotope ratios in pyrite and dissolved sulphate in granitoid fractures down to 1km depth – Evidence for widespread activity of sulphur reducing bacteria, Geochimica et Cosmochimica Acta, 102, 143–161, https://doi.org/10.1016/j.gca.2012.10.036, 2013.

Drake, H., Åström, M. E., Heim, C., Broman, C., Åström, J., Whitehouse, M., Ivarsson, M., Siljeström, S., and Sjövall, P.: Extreme 13C depletion of carbonates formed during oxidation of biogenic methane in fractured granite, Nat Commun, 6, 7020, https://doi.org/10.1038/ncomms8020, 2015a.

Drake, H., Tullborg, E.-L., Whitehouse, M., Sandberg, B., Blomfeldt, T., and Åström, M. E.: Extreme fractionation and micro-scale variation of sulphur isotopes during bacterial sulphate reduction in deep groundwater systems, Geochimica et Cosmochimica Acta, 161, 1–18, https://doi.org/10.1016/j.gca.2015.04.014, 2015b.

Drake, H., Heim, C., Roberts, N. M. W., Zack, T., Tillberg, M., Broman, C., Ivarsson, M., Whitehouse, M. J., and Åström, M. E.: Isotopic evidence for microbial production and consumption of methane in the upper continental crust throughout the Phanerozoic eon, Earth and Planetary Science Letters, 470, 108–118, https://doi.org/10.1016/j.epsl.2017.04.034, 2017.

Drake, H., Whitehouse, M. J., Heim, C., Reiners, P. W., Tillberg, M., Hogmalm, K. J., Dopson, M., Broman, C., and Åström, M. E.: Unprecedented ^{34}S-enrichment of pyrite formed following microbial sulfate reduction in fractured crystalline rocks, Geobiology, 16, 556–574, https://doi.org/10.1111/gbi.12297, 2018.

Drake, H., Roberts, N. M. W., Reinhardt, M., Whitehouse, M., Ivarsson, M., Karlsson, A., Kooijman, E., and Kielman-Schmitt, M.: Biosignatures of ancient microbial life are present across the igneous crust of the Fennoscandian shield, Commun Earth Environ, 2, 102, https://doi.org/10.1038/s43247-021-00170-2, 2021.

Drake, H., Makahnouk, W. R. M., Roberts, N. M. W., Reinhardt, M., Henkemans, E., Frape, S. K., Tullborg, L., Broman, C., Whitehouse, M. J., and Kooijman, E.: Late Cretaceous and Early Paleogene Fluid Circulation and Microbial Activity in Deep Fracture Networks of the Precambrian Basement of Western Greenland, Geochemistry, Geophysics, Geosystems, 25, e2024GC011646, 2024.

Egger, M., Riedinger, N., Mogollón, J. M., and Jørgensen, B. B.: Global diffusive fluxes of methane in marine sediments, Nature Geosci, 11, 421–425, https://doi.org/10.1038/s41561-018-0122-8, 2018.

Eldridge, D. L., Guo, W., and Farquhar, J.: Theoretical estimates of equilibrium sulfur isotope effects in aqueous sulfur systems: Highlighting the role of isomers in the sulfite and sulfoxylate systems, Geochimica et Cosmochimica Acta, 195, 171–200, https://doi.org/10.1016/j.gca.2016.09.021, 2016.

Farquhar, J., Johnston, D. T., Wing, B. A., Habicht, K. S., Canfield, D. E., Airieau, S., and Thiemens, M. H.: Multiple sulphur isotopic interpretations of biosynthetic pathways: implications for biological signatures in the sulphur isotope record, Geobiology, 1, 27–36, https://doi.org/10.1046/j.1472-4669.2003.00007.x, 2003.

Feng, D., Chen, D., Peckmann, J., and Bohrmann, G.: Authigenic carbonates from methane seeps of the northern Congo fan: Microbial formation mechanism, Marine and Petroleum Geology, 27, 748–756, https://doi.org/10.1016/j.marpetgeo.2009.08.006, 2010.

Fichtner, V., Kirchner, F., Kutzschbach, M., Strauss, H., Tillberg, M., Whitehouse, M., and Drake, H.: Microscale δ^{34}S and δ^{18}O variations of barite as an archive for fluid mixing and microbial sulphur metabolisms in igneous rock aquifers, Isotopes in Environmental and Health Studies, 1–28, https://doi.org/10.1080/10256016.2024.2410293, 2024.

Fritz, P., Basharmal, G. M., Drimmie, R. J., Ibsen, J., and Qureshi, R. M.: Oxygen isotope exchange between sulphate and water during bacterial reduction of sulphate, Chemical Geology: Isotope Geoscience section, 79, 99–105, https://doi.org/10.1016/0168-9622(89)90012-2, 1989.

Glossner, A. W., Gallagher, L. K., Landkamer, L., Figueroa, L., Munakata-Marr, J., and Mandernack, K. W.: Factors controlling the co-occurrence of microbial sulfate reduction and methanogenesis in coal bed reservoirs, International Journal of Coal Geology, 165, 121–132, https://doi.org/10.1016/j.coal.2016.08.012, 2016.

Griffith, E. M. and Paytan, A.: Barite in the ocean – occurrence, geochemistry and palaeoceanographic applications, Sedimentology, 59, 1817–1835, https://doi.org/10.1111/j.1365-3091.2012.01327.x, 2012.

Gustafsson, J. and Drake, H.: Biosignatures of an ancient bedrock- and impact structure-hosted deep biosphere: current knowledge and future perspectives, Discov Geosci, 3, 68, https://doi.org/10.1007/s44288-025-00176-9, 2025.

Habicht, K. S., Gade, M., Thamdrup, B., Berg, P., and Canfield, D. E.: Calibration of Sulfate Levels in the Archean Ocean, Science, 298, 2372–2374, 2002.

Halevy, I., Fike, D. A., Pasquier, V., Bryant, R. N., Wenk, C. B., Turchyn, A. V., Johnston, D. T., and Claypool, G. E.: Sedimentary parameters control the sulfur isotope composition of marine pyrite, Science, 382, 946–951, https://doi.org/10.1126/science.adh1215, 2023.

Hallbeck, L. and Pedersen, K.: Explorative analyses of microbes, colloids, and gases together with microbial modelling – Site description model SDM-Site Laxemar, Swedish Nuclear Fuel and Waste Management Co. (SKB), 2008.

Han, T., Bao, H., Peng, Y., Lu, Z., and Song, Y.: The barite record of the past seawater oxygen isotope composition, Nat Commun, 16, 5018, https://doi.org/10.1038/s41467-025-60309-z, 2025.

Heinonen, A., Andersen, T., Rämö, O. T., and Whitehouse, M.: The source of Proterozoic anorthosite and rapakivi granite magmatism: evidence from combined *in situ* Hf–O isotopes of zircon in the Ahvenisto complex, southeastern Finland, JGS, 172, 103–112, https://doi.org/10.1144/jgs2014-013, 2015.

Herlambang, A., John, C. M., and Drake, H.: Physicochemical Conditions of the Devonian-Jurassic Continental Deep Biosphere Tracked by Carbonate Clumped Isotope Temperatures of Granite-Hosted Carbonate Veins, Geofluids, 2023, 1–10, https://doi.org/10.1155/2023/8445328, 2023.

Hoehler, T. M. and Jørgensen, B. B.: Microbial life under extreme energy limitation, Nat Rev Microbiol, 11, 83–94, https://doi.org/10.1038/nrmicro2939, 2013.

Ivarsson, M., Drake, H., Neubeck, A., Sallstedt, T., Bengtson, S., Roberts, N. M. W., and Rasmussen, B.: The fossil record of igneous rock, Earth-Science Reviews, 210, 103342, https://doi.org/10.1016/j.earscirev.2020.103342, 2020.

Iversen, N. and Jorgensen, B. B.: Anaerobic methane oxidation rates at the sulfate-methane transition in marine sediments from Kattegat and Skagerrak (Denmark)1, Limnology & Oceanography, 30, 944–955, https://doi.org/10.4319/lo.1985.30.5.0944, 1985.

Jørgensen, B. B., Böttcher, M. E., Lüschen, H., Neretin, L. N., and Volkov, I. I.: Anaerobic methane oxidation and a deep H2S sink generate isotopically heavy sulfides in Black Sea sediments, Geochimica et Cosmochimica Acta, 68, 2095–2118, https://doi.org/10.1016/j.gca.2003.07.017, 2004.

Jørgensen, B. B., Findlay, A. J., and Pellerin, A.: The Biogeochemical Sulfur Cycle of Marine Sediments, Front. Microbiol., 10, 849, https://doi.org/10.3389/fmicb.2019.00849, 2019.

Kieft, T. L., Walters, C. C., Higgins, M. B., Mennito, A. S., Clewett, C. F. M., Heuer, V., Pullin, M. J., Hendrickson, S., Van Heerden, E., Sherwood Lollar, B., Lau, M. C. Y., and Onstott, T. C.: Dissolved organic matter compositions in 0.6–3.4 km deep fracture waters, Kaapvaal Craton, South Africa, Organic Geochemistry, 118, 116–131, https://doi.org/10.1016/j.orggeochem.2018.02.003, 2018.

Kiyosu, Y. and Krouse, H. R.: The role of organic acid in the abiogenic reduction of sulfate and the sulfur isotope effect, Geochem. J., 24, 21–27, https://doi.org/10.2343/geochemj.24.21, 1990.

Knittel, K. and Boetius, A.: Anaerobic Oxidation of Methane: Progress with an Unknown Process, Annu. Rev. Microbiol., 63, 311–334, https://doi.org/10.1146/annurev.micro.61.080706.093130, 2009.

Kotelnikova, S.: Microbial production and oxidation of methane in deep subsurface, Earth-Science Reviews, 58, 367–395, https://doi.org/10.1016/S0012-8252(01)00082-4, 2002.

Laaksoharju, M., Smellie, J., Tullborg, E.-L., Gimeno, M., Hallbeck, L., Molinero, J., and Waber, N.: Bedrock hydrogeochemistry Forsmark- Site descriptive modelling - SDM-Site Forsmark, Swedish Nuclear Fuel and Waste Management Co. (SKB), Stockholm, Sweden, 2008.

Leavitt, W. D., Halevy, I., Bradley, A. S., and Johnston, D. T.: Influence of sulfate reduction rates on the Phanerozoic sulfur isotope record, Proc. Natl. Acad. Sci. U.S.A., 110, 11244–11249, https://doi.org/10.1073/pnas.1218874110, 2013.

Lin, Z., Wang, Q., Feng, D., Liu, Q., and Chen, D.: Post-depositional origin of highly 13C-depleted carbonate in the Doushantuo cap dolostone in South China: Insights from petrography and stable carbon isotopes, Sedimentary Geology, 242, 71–79, https://doi.org/10.1016/j.sedgeo.2011.10.009, 2011.

Liseroudi, M. H., Ardakani, O. H., Pedersen, P. K., Stern, R. A., Wood, J. M., and Sanei, H.: Microbial and thermochemical controlled sulfur cycle in the Early Triassic sediments of the Western Canadian Sedimentary Basin, Journal of the Geological Society, 178, jgs2020-175, https://doi.org/10.1144/jgs2020-175, 2021.

Machel, H. G.: Bacterial and thermochemical sulfate reduction in diagenetic settings Ð old and new insights, Sedimentary Geology, 2001.

Machel, H. G., Krouse, H. R., and Sassen, R.: Products and distinguishing criteria of bacterial and thermochemical sulfate reduction, Applied Geochemistry, 10, 373–389, https://doi.org/10.1016/0883-2927(95)00008-8, 1995.

Magnabosco, C., Lin, L.-H., Dong, H., Bomberg, M., Ghiorse, W., Stan-Lotter, H., Pedersen, K., Kieft, T. L., Van Heerden, E., and Onstott, T. C.: The biomass and biodiversity of the continental subsurface, Nature Geosci, 11, 707–717, https://doi.org/10.1038/s41561-018-0221-6, 2018.

McMahon, S. and Parnell, J.: Weighing the deep continental biosphere, FEMS Microbiol Ecol, 87, 113–120, https://doi.org/10.1111/1574-6941.12196, 2014.

McMahon, S. and Parnell, J.: The deep history of Earth's biomass, JGS, 175, 716–720, https://doi.org/10.1144/jgs2018-061, 2018.

Mizutani, Y. and Rafter, T. A.: Isotopic behaviour of sulphate oxygen in the bacterial reduction of sulphate, Geochemical Journal, 6, 183–191, 1973.

Natalicchio, M., Birgel, D., Dela Pierre, F., Martire, L., Clari, P., Spötl, C., and Peckmann, J.: Polyphasic carbonate precipitation in the shallow subsurface: Insights from microbially-formed authigenic carbonate beds in upper Miocene sediments of the Tertiary Piedmont Basin (NW Italy), Palaeogeography, Palaeoclimatology, Palaeoecology, 329–330, 158–172, https://doi.org/10.1016/j.palaeo.2012.02.026, 2012.

Osterholz, H., Turner, S., Alakangas, L. J., Tullborg, E.-L., Dittmar, T., Kalinowski, B. E., and Dopson, M.: Terrigenous dissolved organic matter persists in the energy-limited deep groundwaters of the Fennoscandian Shield, Nature Communications, 13, 4837, 2022.

Paiste, K., Fike, D. A., Kirsimäe, K., Jones, C., and Lepland, A.: Testing the global significance of the sulfur isotope record of the ca. 2.0 Ga Zaonega Formation: A micro-scale S isotope investigation, Geochimica et Cosmochimica Acta, 331, 86–104, https://doi.org/10.1016/j.gca.2022.05.021, 2022.

Pallud, C. and Van Cappellen, P.: Kinetics of microbial sulfate reduction in estuarine sediments, Geochimica et Cosmochimica Acta, 70, 1148–1162, https://doi.org/10.1016/j.gca.2005.11.002, 2006.

Pasquier, V., Marin-Carbonne, J., Giunta, T., Ruffine, L., and Halevy, I.: Microscale iron and sulphur isotopic compositions reveal pyritization pathways during early diagenesis, Commun Earth Environ, 6, 248, https://doi.org/10.1038/s43247-025-02213-4, 2025.

Paytan, A., Kastner, M., Campbell, D., and Thiemens, M. H.: Sulfur Isotopic Composition of Cenozoic Seawater Sulfate, Science, 282, 1459–1462, https://doi.org/10.1126/science.282.5393.1459, 1998.

Paytan, A., Mearon, S., Cobb, K., and Kastner, M.: Origin of marine barite deposits: Sr and S isotope characterization, Geol, 30, 747, https://doi.org/10.1130/0091-7613(2002)030%3C0747:OOMBDS%3E2.0.CO;2, 2002.

Pedersen, K., Ekendahl, S., Tullborg, E.-L., Furnes, H., Thorseth, I., and Tumyr, O.: Evidence of ancient life at 207 m depth in a granitic aquifer, Geology, 25, 827–830, 1997.

Pedregosa, F., Varoquaux, G., Gramfort, A., Michel, V., Thirion, B., Grisel, O., Blondel, M., Prettenhofer, P., Weiss, R., Dubourg, V., Vanderplas, J., Passos, A., Brucher, M., Perrot, M., and Duchesnay, É.: Scikit-learn: Machine Learning in Python, Journal of Machine Learning Research, 12, 2825–2830, 2011.

Reeburgh, W. S.: Oceanic Methane Biogeochemistry, Chem. Rev., 107, 486–513, https://doi.org/10.1021/cr050362v, 2007.

Reitner, J., Peckmann, J., Reimer, A., Schumann, G., and Thiel, V.: Methane-derived carbonate build-ups and associated microbial communities at cold seeps on the lower Crimean shelf (Black Sea), Facies, 51, 66–79, https://doi.org/10.1007/s10347-005-0059-4, 2005.

Ries, J. B., Fike, D. A., Pratt, L. M., Lyons, T. W., and Grotzinger, J. P.: Superheavy pyrite (δ34Spyr > δ34SCAS) in the terminal Proterozoic Nama Group, southern Namibia: A consequence of low seawater sulfate at the dawn of animal life, Geology, 37, 743–746, https://doi.org/10.1130/G25775A.1, 2009.

Roychoudhury, A. N., Van Cappellen, P., Kostka, J. E., and Viollier, E.: Kinetics of microbially mediated reactions: dissimilatory sulfate reduction in saltmarsh sediments (Sapelo Island, Georgia, USA), Estuarine, Coastal and Shelf Science, 56, 1001–1010, https://doi.org/10.1016/S0272-7714(02)00325-6, 2003.

Rudnicki, M. D., Elderfield, H., and Spiro, B.: Fractionation of sulfur isotopes during bacterial sulfate reduction in deep ocean sediments at elevated temperatures, Geochimica et Cosmochimica Acta, 65, 777–789, https://doi.org/10.1016/S0016-7037(00)00579-2, 2001.

Ruff, S. E., De Angelis, I. H., Mullis, M., Payet, J. P., Magnabosco, C., Lloyd, K. G., Sheik, C. S., Steen, A. D., Shipunova, A., Morozov, A., Reese, B. K., Bradley, J. A., Lemonnier, C., Schrenk, M. O., Joye, S. B., Huber, J. A., Probst, A. J., Morrison, H. G., Sogin, M. L., Ladau, J., and Colwell, F.: A global comparison of surface and subsurface microbiomes reveals large-scale biodiversity gradients, and a marine-terrestrial divide, Sci. Adv., 10, eadq0645, https://doi.org/10.1126/sciadv.adq0645, 2024.

Runge, E. A., Mansor, M., Kappler, A., and Duda, J.-P.: Microbial biosignatures in ancient hydrothermal sulfides, Geobiology, 21, 355–377, 2023.

Schidlowski, M.: Carbon isotopes as biogeochemical recorders of life over 3.8 Ga of Earth history: evolution of a concept, Precambrian Research, 106, 117–134, https://doi.org/10.1016/S0301-9268(00)00128-5, 2001.

Sela-Adler, M., Ronen, Z., Herut, B., Antler, G., Vigderovich, H., Eckert, W., and Sivan, O.: Co-existence of Methanogenesis and Sulfate Reduction with Common Substrates in Sulfate-Rich Estuarine Sediments, Front. Microbiol., 8, 766, https://doi.org/10.3389/fmicb.2017.00766, 2017.

Sim, M. S., Bosak, T., and Ono, S.: Large Sulfur Isotope Fractionation Does Not Require Disproportionation, Science, 333, 74–77, https://doi.org/10.1126/science.1205103, 2011.

Sim, M. S., Woo, D. K., Kim, B., Jeong, H., Joo, Y. J., Hong, Y. W., and Choi, J. Y.: What Controls the Sulfur Isotope Fractionation during Dissimilatory Sulfate Reduction?, ACS Environ. Au, 3, 76–86, https://doi.org/10.1021/acsenvironau.2c00059, 2023.

Stevens, T. O. and McKinley, J. P.: Lithoautotrophic Microbial Ecosystems in Deep Basalt Aquifers, Science, 270, 450–455, https://doi.org/10.1126/science.270.5235.450, 1995.

Strauss, H.: The isotopic composition of sedimentary sulfur through time, Palaeogeography, Palaeoclimatology, Palaeoecology, 132, 97–118, 1997.

Takai, K., Nakamura, K., Toki, T., Tsunogai, U., Miyazaki, M., Miyazaki, J., Hirayama, H., Nakagawa, S., Nunoura, T., and Horikoshi, K.: Cell proliferation at 122°C and isotopically heavy CH_4 production by a hyperthermophilic methanogen under high-pressure cultivation, Proc. Natl. Acad. Sci. U.S.A., 105, 10949–10954, https://doi.org/10.1073/pnas.0712334105, 2008.

https://doi.org/10.5194/egusphere-2026-2220
Preprint. Discussion started: 23 April 2026

Torres, M. E., Brumsack, H. J., Bohrmann, G., and Emeis, K. C.: Barite fronts in continental margin sediments: a new look at barium remobilization in the zone of sulfate reduction and formation of heavy barites in diagenetic fronts, Chemical Geology, 127, 125–139, https://doi.org/10.1016/0009-2541(95)00090-9, 1996.

Turchyn, A. V. and Schrag, D. P.: Oxygen Isotope Constraints on the Sulfur Cycle over the Past 10 Million Years, Science, 303, 2004–2007, https://doi.org/10.1126/science.1092296, 2004.

Turchyn, A. V. and Schrag, D. P.: Cenozoic evolution of the sulfur cycle: Insight from oxygen isotopes in marine sulfate, Earth and Planetary Science Letters, 241, 763–779, https://doi.org/10.1016/j.epsl.2005.11.007, 2006.

Whitehouse, M. J.: Multiple Sulfur Isotope Determination by SIMS : Evaluation of Reference Sulfides for Δ^{33} S with Observations and a Case Study on the Determination of Δ^{36} S, Geostandard Geoanalytic Res, 37, 19–33, https://doi.org/10.1111/j.1751-908X.2012.00188.x, 2013.

Whiticar, M. J.: Carbon and hydrogen isotope systematics of bacterial formation and oxidation of methane, Chemical Geology, 161, 291–314, https://doi.org/10.1016/S0009-2541(99)00092-3, 1999.

Wing, B. A. and Halevy, I.: Intracellular metabolite levels shape sulfur isotope fractionation during microbial sulfate respiration, Proc. Natl. Acad. Sci. U.S.A., 111, 18116–18125, https://doi.org/10.1073/pnas.1407502111, 2014.

Wood, R. S., Lepland, A., Ogliore, R. C., Houghton, J., and Fike, D. A.: Microscale δ34S heterogeneities in cold seep barite record variable methane flux off the Lofoten-Vesterålen Continental Margin, Norway, Earth and Planetary Science Letters, 574, 117164, https://doi.org/10.1016/j.epsl.2021.117164, 2021.

Wortmann, U. G., Bernasconi, S. M., and Böttcher, M. E.: Hypersulfidic deep biosphere indicates extreme sulfur isotope fractionation during single-step microbial sulfate reduction, Geol, 29, 647, https://doi.org/10.1130/0091-7613(2001)029%3C0647:HDBIES%3E2.0.CO;2, 2001.

Wortmann, U. G., Chernyavsky, B., Bernasconi, S. M., Brunner, B., Böttcher, M. E., and Swart, P. K.: Oxygen isotope biogeochemistry of pore water sulfate in the deep biosphere: Dominance of isotope exchange reactions with ambient water during microbial sulfate reduction (ODP Site 1130), Geochimica et Cosmochimica Acta, 71, 4221–4232, https://doi.org/10.1016/j.gca.2007.06.033, 2007.

Wu, X., Holmfeldt, K., Hubalek, V., Lundin, D., Åström, M., Bertilsson, S., and Dopson, M.: Microbial metagenomes from three aquifers in the Fennoscandian shield terrestrial deep biosphere reveal metabolic partitioning among populations, The ISME Journal, 10, 1192–1203, https://doi.org/10.1038/ismej.2015.185, 2016.

Yang, L. W., Yang, T., Li, J., Lin, Y., and Ling, H.-F.: The marine redox evolution and the formation model for the early Cambrian Gongxi-Tianzhu barite deposits in the South China Block, Ore Geology Reviews, 158, 105502, https://doi.org/10.1016/j.oregeorev.2023.105502, 2023.

Zaback, D. A., Pratt, L. M., and Hayes, J. M.: Transport and reduction of sulfate and immobilization of sulfide in marine black shales, Geol, 21, 141, https://doi.org/10.1130/0091-7613(1993)021%3C0141:TAROSA%3E2.3.CO;2, 1993.

Zan, B., Mou, C., Lash, G. G., Yan, J., and Hou, Q.: Diagenetic barite-calcite-pyrite nodules in the Silurian Longmaxi Formation of the Yangtze Block, South China: A plausible record of sulfate-methane transition zone movements in ancient marine sediments, Chemical Geology, 595, 120789, https://doi.org/10.1016/j.chemgeo.2022.120789, 2022.

Zhou, X., Chen, D., Dong, S., Zhang, Y., Guo, Z., Wei, H., and Yu, H.: Diagenetic barite deposits in the Yurtus Formation in Tarim Basin, NW China: Implications for barium and sulfur cycling in the earliest Cambrian, Precambrian Research, 263, 79–87, https://doi.org/10.1016/j.precamres.2015.03.006, 2015.